PHYSICAL REVIEW E **92**, 023307 (2015)

Assessment of interaction potential in simulating nonisothermal multiphase systems by means of lattice Boltzmann modeling

Ahad Zarghami,[*] Niels Looije, and Harry Van den Akker
Transport Phenomena Group, Department of Chemical Engineering, TU Delft, The Netherlands

(Received 18 May 2015; published 26 August 2015)

The pseudopotential lattice Boltzmann model (PP-LBM) is a very popular model for simulating multiphase systems. In this model, phase separation occurs via a short-range attraction between different phases when the interaction potential term is properly chosen. Therefore, the potential term is expected to play a significant role in the model and to affect the accuracy and the stability of the computations. The original PP-LBM suffers from some drawbacks such as being capable of dealing with low density ratios only, thermodynamic inconsistency, and spurious velocities. In this paper, we aim to analyze the PP-LBM with the view to simulate single-component (non-)isothermal multiphase systems at large density ratios and in spite of the presence of spurious velocities. For this purpose, the performance of two popular potential terms and of various implementation schemes for these potential terms is examined. Furthermore, the effects of different parameters (i.e., equation of state, viscosity, etc.) on the simulations are evaluated, and, finally, recommendations for a proper simulation of (non-)isothermal multiphase systems are presented.

DOI: 10.1103/PhysRevE.92.023307 PACS number(s): 47.55.−t, 47.11.−j, 02.70.−c, 68.03.−g

I. INTRODUCTION

Multiphase flows are very common in many engineering systems, such as gas-liquid flows in evaporators and condensers, boilers, and heat pipes. Multiphase flows also are abundantly present in nature, like rain, clouds, fog, avalanches, and blood flow. Due to the obvious importance of multiphase flows, many numerical models were developed to study and simulate the various flow regimes possible, in particular the dispersed regimes of bubbles and drops. In the latter cases, the real challenge is in capturing or tracking the interface between phases which result from phase separation due to the physicochemical interactions among the constituent molecules.

The common models based on the Navier-Stokes (NS) equations are divided into interface (or front) tracking and capturing categories. In interface tracking methods, the interface is defined as boundary condition and is tracked directly in each time step. The most popular interface-tracking methods are the boundary-fitted grid method [1], the Tryggvasson's hybrid method [2], and the boundary element method (BEM) [3]. Usually, the interface tracking methods allow us to accurately calculate the interface curvature; however, these methods need complex boundary models and complicated dynamic meshing algorithms. These limitations are alleviated by using interface-capturing methods such as the marker-and-cell (MAC) method [4], the volume-of-fluid (VOF) method [5], and the level set (LS) method [6]. In these methods, all phases and components of the flow are modeled as single continuous media with discontinuous properties at the interface. Solving the full NS equations with a coupled algorithm to simultaneously resolve the interface is the main complexity of these methods which has limited them to relatively simple cases [7]. Generally, tracking or capturing the interface and generating a dynamic mesh are always a challenging issue, especially for rapidly transient cases, for high-density-ratio flows, and in problems with complex geometries [8].

As mentioned before, phase separation and forming the interface are the consequence of molecular interactions. The effects of these molecular interactions on multiphase flows are ignored in traditional NS-based methods as they are purely continuum-based techniques. Therefore, there is a necessity for alternative techniques to comprehend the connection between the macroscopic phenomena and the underlying microscopic interactions. In principle, atomistic methods such as molecular dynamics (MD) or direct simulation Monte Carlo (DSMC) are suitable for capturing the microscopic interactions. However, these techniques are computationally too challenging to be applied to macroscopic engineering problems. Over the past three decades, the lattice Boltzmann method (LBM), which is based on a mesoscopic kinetic equation for particle distribution functions, has been introduced as an alternative and feasible tool for simulating multiphase flows [9–13].

There are a number of approaches for simulating multiphase flows by using LBM: the color-gradient model [9], the index fluid method [10], the free-energy model [11], and the pseudopotential multiphase LBM proposed by Shan and Chen [12,13]. All these approaches have their origins in kinetic theory, but the last two models have shown the most promise and capability for simulating multiphase systems. The free energy model relies on the incorporation of nonequilibrium dynamics by using the concept of a free energy function. This model is physically consistent and conserves local momentum. However, Galilean invariance is not satisfied, some unphysical effects have been noted in simulations, and the method is limited by the admissible range of fluid properties (density ratio, surface tension, and kinematic viscosity), time and length scales, and by the inability to represent energy transport [14].

The PP-LBM (also called the Shan-Chen or SC model) is a very popular model in the LB community. In this model, the fluid interactions are mimicked by an interparticle potential; consequently, the interaction potentials produce the form of the equation of state (EOS) of the fluid. Phase separation occurs via

---

[*] Present address: Department of Chemical Eng., TU Delft, Julianalaan 136, 2628BL Delft, Netherlands; a.zarghami-1@tudelft.nl

a short-range attraction between the various phases when the interaction potentials are properly chosen. In this model, the interface is captured automatically and molecular interactions are incorporated as the driving force behind phase separation. Hou *et al.* [15] demonstrated that, in comparison with the free-energy model, the PP-LBM is more stable and has more accurate results. Yu and Fan [16] extended the PP-LBM to a multiple-relaxation-time version and showed that their model is able to significantly enhance the numerical stability at low viscosities. A critical review of the theory and applications of the PP-LBM in the simulation of multiphase flows during the past two decades has been presented in Ref. [17].

In practical problems, density ratios between phases can vary greatly. For example, the density ratio of a liquid emulsion is of the $O(1)$, while the density ratio of a water-air system can be higher than $O(1000)$. The original PP-LBM [12] can be used to simulate a system with a density ratio of the $O(10)$, but the simulation fails for higher density ratio systems due to the generation of either an infinitely large or a negative density [8]. A low density ratio indeed prevents the PP-LBM model from being applied to many multiphase flow systems. For the sake of overcoming this drawback, different researchers tried to develop the original PP-LBM for high-density-ratio simulations by incorporating a proper realistic EOS in the original model [8,18,19].

In addition to the low density ratio, the original PP-LBM suffers from a thermodynamic inconsistency and large spurious velocities [20]. In thermodynamic theory, the coexistent densities for multiphase flows are determined by the Maxwell construction. However, the coexistent densities obtained by the original PP-LBM are inconsistent with the Maxwell construction and the inconsistency increases when operating too far below the critical temperature. The spurious velocities denote vortexlike fluid velocities, which are formed in the vicinity of a curved phase interface. These spurious velocities are a common problem for many multiphase flow models, as interface dynamics and transport phenomena across an interface are seriously affected by them [20]. The amplitude of the spurious velocities increases as the density ratio goes up, which causes numerical instability and limits the maximum density ratios achievable [17]. The spurious velocities can be reduced by extending the spatial range of the pseudopotential interaction [20,21]. Also, it has been shown that the thermodynamic inconsistency can be controlled by a proper implementation of a suitable EOS in the model [19,22,23]. This is achieved by a proper approximation of the potential gradient and also selecting an accurate force implementation strategy [19,24,25].

Notwithstanding the great efforts made to study the hydrodynamics of multiphase flows [19–31], modeling thermal multiphase systems at large density ratios is still very challenging, because many issues should be addressed simultaneously. The motivation of the present work is to extend the PP-LBM to simulate (non-)isothermal multiphase systems at large density ratio in spite of the presence of spurious velocities. In this paper, we aim to address these issues through a proper assessment of specific potential terms in the PP-LBM which have been proposed in the literature to incorporate attractive (or repulsive) forces between different phases. Here we present a straightforward and comprehensive analysis of two popular schemes, i.e., the Shan-Chen potential [12] and the so-called β-potential terms [23]. By carrying out this analysis, the effect of spurious velocities on the temperature domain is investigated and the effects of different parameters on the simulations are evaluated and, finally, recommendations for a proper simulation are presented.

The rest of the present paper is organized as follows: The numerical model is presented in Sec. II. In this section, the details of interaction potential terms, forcing implementation schemes, and incorporating equation of states are presented comprehensively. The numerical results are presented in Sec. III and, finally, concluding remarks are given in Sec. IV.

II. NUMERICAL METHOD

In this section, the details of numerical methods to solve a single-component multiphase system are presented. We first recall the thermal LBM; then details of two alternative potential terms for simulating multiphase syetsms, various force implementation schemes, and EOSs are presented.

A. Thermal LBM

The general lattice Boltzmann equation with a single relaxation time is written as [12,32]:

$$f_i(\vec{x}+\vec{e}_i\Delta t,t+\Delta t)-f_i(\vec{x},t) = -\frac{1}{\tau}\left[f_i(\vec{x},t)-f_i^{\mathrm{eq}}(\vec{x},t)\right]+S_i, \tag{1}$$

where f_i is the kinetic probability density function and f_i^{eq} is the equilibrium distribution, corresponding to the Maxwellian distribution in the continuum limit [20]. Also, τ is the nondimensional relaxation time and S_i represents a general source term added to the standard lattice Boltzmann equation. The discrete velocities $\vec{e}_i$ in the ith direction for the D$_2$Q$_9$ lattice are given by $\vec{e}_0 = 0$ and $\vec{e}_i = \lambda_i(\cos\theta_i, \sin\theta_i)$ with $\lambda_i = 1, \theta_i = (i-1)\pi/2$ for $i = 1 \sim 4$ and $\lambda_i = \sqrt{2}, \theta_i = (i-5)\pi/2 + \pi/4$ for $i = 5 \sim 8$. The order numbers $i = 1 \sim 4$ and $i = 5 \sim 8$ represent the rectangular and the diagonal directions of the lattice, respectively. The equilibrium density distribution functions, f_i^{eq}, are obtained via a low-Mach-number expansion of the continuum Maxwellian are given by:

$$f_i^{\mathrm{eq}} = w_i\rho\left[1+\frac{(\vec{e}_i\cdot\vec{u}^{\mathrm{eq}})}{c_s^2}+\frac{(\vec{e}_i\cdot\vec{u}^{\mathrm{eq}})^2}{2c_s^4}-\frac{(\vec{u}^{\mathrm{eq}}\cdot\vec{u}^{\mathrm{eq}})}{2c_s^2}\right]_{i=1\sim 9}, \tag{2}$$

where $c_s = c/\sqrt{3}$ denotes the lattice speed of sound and $c = \Delta x/\Delta t$ is the lattice speed with Δx and Δt as the lattice spacing and time interval (both Δx and Δt are equal to 1 in the lattice system). Also, w_i's are the weighting factors, equal to 4/9 for $i = 0$, 1/9 for $i = 1 \sim 4$, and 1/36 for $i = 5 \sim 8$, and $\vec{u}^{\mathrm{eq}}$ is the equilibrium velocity. The local mass density, the local velocity, and the viscosity in lattice units are calculated as $\rho = \sum_i f_i$, $\vec{u} = (\sum_i \vec{e}_i f_i)/\rho$, and $\nu = c_s^2(\tau - 0.5)$, respectively. Hence, the viscosity can be changed by choosing a different relaxation time.

Similarly, by introducing a second distribution function and when ignoring the viscous dissipation term, a thermal LBM is obtained:

$$g_i(\vec{x}+\vec{e}_i\Delta t,t+\Delta t)-g_i(\vec{x},t) = -\frac{1}{\tau_g}\left[g_i(\vec{x},t)-g_i^{\mathrm{eq}}(\vec{x},t)\right]+w_i\Lambda, \tag{3}$$

where the g_i's are the energy distribution functions along the particle velocity directions, τ_{g} is the thermal relaxation time, and g_i^{eq} denotes the energy distribution equilibrium functions given by:

$$g_i^{\mathrm{eq}} = w_i\rho T\left[1+\frac{\vec{e}_i\cdot\vec{U}}{c_s^2}\right]_{i=1\sim 9}, \tag{4}$$

where $\vec{U}$ is the macroscopic velocity, Λ is the energy source term, and $T=\sum_i g_i/\rho$ is the temperature. In order to mimic the macroscopic energy equation, the energy source term should be defined as [31]:

$$\Lambda = \frac{\nabla\cdot(k\nabla T)}{c_p}-\nabla\cdot[\alpha\nabla(\rho T)], \tag{5}$$

where k is thermal conductivity, c_p is specific heat, and $\alpha = c_s^2(\tau_g-0.5)$ is thermal diffusivity. Therefore, by implementing the Chapman-Enskog expansion, the macroscopic energy equation for multiphase flows is recovered as:

$$\frac{\partial T}{\partial t}+\vec{U}\cdot\nabla T = \frac{\nabla\cdot(k\nabla T)}{\rho c_p}. \tag{6}$$

B. Interaction potential for multiphase systems

The force acting on a multiphase system includes external body forces, $\vec{F}_{\mathrm{body}}$ (e.g., gravity), and the mean field interparticle interaction potential (or force), $\vec{F}_{\mathrm{potential}}$ and is written as: $\vec{F}=\vec{F}_{\mathrm{body}}+\vec{F}_{\mathrm{potential}}$. In this work, the external body forces are neglected and therefore, $\vec{F}=\vec{F}_{\mathrm{potential}}$. This interparticle interaction potential accounts for the phase separation in the PP-LBM [12,33]. In the following, we review two existing schemes for interparticle interaction potential terms.

1. *The Shan-Chen potential term*

In a multiphase system, part of the interaction force acts between molecules in the same phase, while another part acts between molecules in different phases. Based on the original PP-LBM proposed by Shan and Chen [12,13], the interaction force for a single-component multiphase system is written as:

$$\vec{F}_{\mathrm{potential,SC}} = -G\psi(\vec{x},t)\sum_i w_i\vec{e}_i\psi(\vec{x}+\vec{e}_i,t), \tag{7}$$

where G denotes the interaction parameter, with $G<0$ representing an attractive force and $G>0$ representing a repulsive force between particles. Also, $\psi(\vec{x},t)$ is called the effective mass or the pseudopotential function, which is a function of local density and describes the fluid-fluid interactions triggered by inhomogeneities of the density profile. Here the interaction is restricted to nearest and next-nearest neighbors. The original form of $\psi(\vec{x},t)$ is defined as:

$$\psi(\vec{x},t)=\rho_0(1-\exp^{-\rho/\rho_0}), \tag{8}$$

where ρ_0 is a normalization constant, which is usually chosen as 1. The EOS corresponding to Eq. (7) is named Shan-Chen EOS and is presented as [12,13]:

$$p_{\mathrm{SC}}=\rho c_s^2+\frac{G}{2}c_s^2[\psi(\vec{x},t)]^2, \tag{9}$$

For the potential form in Eq. (8), a van der Waals-type of EOS is retrieved. As we mentioned in earlier, incorporating a proper attainable EOS in the model leads to reduction in spurious velocities and increases the density ratios attainable [18]. In the framework of the isothermal LBM, a relatively simple but effective method for incorporating various EOS into the original PP-LBM was obtained by rewriting Eq. (8) as [18,34,35]:

$$\psi(\vec{x},t)=\sqrt{\frac{2\left(p_{\mathrm{EOS}}-\rho c_s^2\right)}{Gc_s^2}}, \tag{10}$$

where p_{EOS} is the pressure. With this method, any EOS can be incorporated in the interparticle interaction force through Eq. (10). Hence, different EOSs would give different interparticle interaction forces. Note that for the single-component multiphase simulations, the value of G becomes unimportant and is canceled out of the computations.

2. *The β-scheme potential term*

By considering Eq. (7), we can realize that the determination of the neighbor nodes has a great role in the calculation of the force term. In the Shan-Chen potential term [Eq. (7)], only the nearest and next-nearest neighbors are considered. It has been demonstrated that the relatively large spurious velocities in the vicinity of the curved interface in the model result from insufficient isotropy of the interaction force. By increasing the isotropy, the magnitude of spurious velocities decreases, the thermodynamic inconsistency reduces, and the stable temperature range extends [19,20,23,36].

Since finite sets of discrete velocities $\vec{e}_i$ are defined in LBM, it is not possible to have a fully isotropic force. For a two-dimensional case with nearest and next-nearest neighbors, only an isotropy up to fourth order can be achieved. However, if the next layers of neighboring nodes are taken into account, the order of the isotropy increases at the expense of an increase in computational cost [20,36].

The consequence of the interaction potential of Eq. (7) at the continuum limit is achieved by letting the lattice scale approach zero [37]. By implementing a Taylor expansion of the interaction potential, Eq. (7) is then rewritten as:

$$\vec{F}_{\mathrm{potential}}=-G\left[\psi\nabla\psi+\frac{\varepsilon}{2}\psi\nabla(\nabla^2\psi)+\cdots\right], \tag{11}$$

where ε is the expansion parameter, which is proportional to the ratio of the lattice spacing to a characteristic macroscopic length. Equation (11) shows that the interaction potential is defined as function of the gradient and higher derivatives of the density field and should include any number of neighbor nodes for obtaining a higher degree of isotropy. If we ignore the higher order terms in Eq. (11) and represent the first term in the right-hand side as $-\psi\nabla\psi=-0.5\nabla(\psi)^2$, the interaction potential term can be alternatively calculated as:

$$\vec{F}_{\text{potential}} = -0.5G \sum_i w_i [\psi(\vec{x} + \vec{e}_i, t)]^2 \vec{e}_i \qquad (12)$$

The above equation involves the effective mass of nearest and next-nearest lattices. Gong and Cheng [23,38] found that the combination of Eqs. (7) and (12) can increase the isotropy of the interaction force. The new potential term, which is the so-called β-scheme potential term, is written as follows:

$$\vec{F}_{\text{potential},\beta} = -\beta\left[\psi(\vec{x},t) G \sum_i w_i \vec{e}_i \psi(\vec{x} + \vec{e}_i, t)\right] - \frac{1-\beta}{2}\left[G \sum_i w_i \vec{e}_i \psi(\vec{x} + \vec{e}_i, t)^2\right], \qquad (13)$$

where β is the weighting factor. In fact, rather than considering more neighboring nodes to increase the isotropy, the force and, consequently, the surface tension are tunable and we can reach to the optimum fourth-order isotropic solution for the case with nearest and next-nearest neighbors [23,38]. By choosing a proper value for β, the thermodynamic inconsistency and magnitude of spurious velocities reduce greatly [23]. For $\beta = 1$, the scheme coincides with Eq. (7), for $\beta = 0$, with Eq. (12).

C. Force implementation scheme

In order to mimic the continuous phase behavior as expressed by the NS equations, usually, a source term taking care of the mean-field interparticle interaction force is added to the LBE [see Eq. (1)]. Different implementation schemes have been presented in the literature to include this force term in LBM. Selecting a proper method has a great effect on the numerical stability and accuracy of the solution. In this section, we introduce the most popular implementation schemes.

1. The Shan-Chen scheme

In this scheme, also called the velocity shifting method, the incorporation of the force term is realized by means of a shifted equilibrium velocity $\vec{u}^{\text{eq}}$ when calculating the equilibrium distribution function [12]. In other words, the equilibrium velocity in Eq. (2) is calculated as:

$$\vec{u}^{\text{eq}} = \vec{u} + \frac{\tau}{\rho}\vec{F}. \qquad (14)$$

Due to averaging the momentum before and after the collision step, the actual fluid velocity is calculated as:

$$\vec{U} = \vec{u} + \frac{\Delta t}{2\rho}\vec{F}. \qquad (15)$$

The equivalent macroscopic NS equations corresponding to this scheme are obtained as:

$$\frac{\partial\rho}{\partial t} + \nabla\cdot(\rho\vec{U}) = -\frac{\Delta t}{2}\nabla\cdot\vec{F} \qquad (16a)$$

$$\frac{\partial}{\partial t}(\rho\vec{U}) + \nabla\cdot(\rho\vec{U}\vec{U}) = -\nabla p + \nu\nabla\cdot[\rho(\nabla\vec{U} + (\nabla\vec{U})^T)] + \vec{F} \underbrace{-\frac{\Delta t}{2}\varepsilon\frac{\partial\vec{F}}{\partial t_1} - \Delta t\nabla\cdot\left[\frac{1}{2}(\vec{U}\vec{F} + \vec{F}\vec{U}) + \frac{\tau^2}{\rho}\vec{F}\vec{F}\right]}_{\vec{F}_{\text{extra}}} \qquad (16b)$$

It is clear that the macroscopic NS equations recovered from the Shan-Chen force implementation scheme contain additional terms.

2. The He scheme

He *et al.* [39] proposed another idea to incorporate force into the LBM. In their scheme the discrete form of the force is written as:

$$S_i = w_i\left[\frac{\vec{e}_i - \vec{u}}{c_s^2} + \frac{(\vec{e}_i\cdot\vec{u})}{c_s^4}\vec{e}_i\right]\cdot\vec{F}\Delta t, \qquad (17)$$

where the equilibrium and the real velocity of the fluid are defined as $\vec{u} = \vec{u}^{\text{eq}} = \vec{U} = \sum \vec{e}_i f_i/\rho$. Using this scheme, the macroscopic NS equations are given by:

$$\frac{\partial\rho}{\partial t} + \nabla\cdot(\rho\vec{U}) = -\frac{\Delta t}{2}\nabla\cdot\vec{F}, \qquad (18a)$$

$$\frac{\partial}{\partial t}(\rho\vec{U}) + \nabla\cdot(\rho\vec{U}\vec{U}) = -\nabla p + \nu\nabla\cdot[\rho(\nabla\vec{U} + (\nabla\vec{U})^T)] + \vec{F} \underbrace{-\frac{\Delta t}{2}\varepsilon\frac{\partial\vec{F}}{\partial t_1} - \left(\tau - \frac{1}{2}\right)\Delta t\nabla\cdot[\vec{U}\vec{F} + \vec{F}\vec{U}]}_{\vec{F}_{\text{extra}}}. \qquad (18b)$$

It can be seen that the macroscopic equations recovered from the He scheme contain the additional term $\vec{F}_{\text{extra}}$.

3. The BG scheme

Buick and Greated [40] proposed a method for introducing a force, in the incompressible limit, into the LBM. In this method, the discrete form of the force is as:

$$S_i = \left(1 - \frac{1}{2\tau}\right) w_i \left[\frac{\vec{e}_i}{c_s^2}\right] \cdot \vec{F} \Delta t, \tag{19}$$

where the macroscopic and the equilibrium velocities are defined the same as in Eq. (15). The resulting macroscopic NS equations derived from this method are as follows:

$$\frac{\partial \rho}{\partial t} + \nabla \cdot (\rho \vec{U}) = 0, \tag{20a}$$

$$\frac{\partial}{\partial t}(\rho \vec{U}) + \nabla \cdot (\rho \vec{U}\vec{U}) = -\nabla p + \nu \nabla \cdot [\rho(\nabla \vec{U} + (\nabla \vec{U})^T)] + \vec{F} + \underbrace{\left(\tau - \frac{1}{2}\right)\Delta t \nabla \cdot [\vec{U}\vec{F} + \vec{F}\vec{U}]}_{\vec{F}_{\text{extra}}}. \tag{20b}$$

It is clear that the momentum equation differs from the true NS equation by an additional term $\vec{F}_{\text{extra}}$.

4. The Guo scheme

This scheme was proposed by Guo *et al.* [41]. Using this scheme, the discrete form of the force is written in a power series form as:

$$S_i = \left(1 - \frac{1}{2\tau}\right) w_i \left[\frac{\vec{e}_i - \vec{u}^{\text{eq}}}{c_s^2} + \frac{(\vec{e}_i \cdot \vec{u}^{\text{eq}})}{c_s^4}\vec{e}_i\right] \cdot \vec{F} \Delta t, \tag{21}$$

where the macroscopic and the equilibrium velocity are defined the same as in Eq. (15). By substituting Eq. (21) into (1) and implementing the Chapman-Enskog expansion, the NS equations are recovered as:

$$\frac{\partial \rho}{\partial t} + \nabla \cdot (\rho \vec{U}) = 0, \tag{22a}$$

$$\frac{\partial}{\partial t}(\rho \vec{U}) + \nabla \cdot (\rho \vec{U}\vec{U}) = -\nabla p + \nu \nabla \cdot [\rho(\nabla \vec{U} + (\nabla \vec{U})^T)] + \vec{F}. \tag{22b}$$

It is obvious that the Guo scheme exactly matches the NS equations.

5. The EDM scheme

The exact difference method (EDM) was directly derived from the Boltzmann equation by Kupershtokh *et al.* [19]. In this scheme, the force term in Eq. (1) is obtained by:

$$S_i = f_i^{\text{eq}}(\rho, \vec{u} + \vec{F}\Delta t/\rho) - f_i^{\text{eq}}(\rho, \vec{u}). \tag{23}$$

Here S_i is the difference between the equilibrium distribution functions corresponding to the velocity after and before the action of particle interaction force. In this method, the equilibrium velocity is expressed in the same form of $\vec{u}$ and the real fluid velocity is calculated by Eq. (15). The macroscopic NS equations recovered from the EDM scheme are:

$$\frac{\partial \rho}{\partial t} + \nabla \cdot (\rho \vec{U}) = -\frac{\Delta t}{2} \nabla \cdot \vec{F}, \tag{24a}$$

$$\frac{\partial}{\partial t}(\rho \vec{U}) + \nabla \cdot (\rho \vec{U}\vec{U}) = -\nabla p + \nu \nabla \cdot [\rho(\nabla \vec{U} + (\nabla \vec{U})^T)] + \vec{F} \underbrace{- \frac{\Delta t}{2}\varepsilon \frac{\partial \vec{F}}{\partial t_1} - \Delta t \nabla \cdot \left[\frac{1}{2}(\vec{U}\vec{F} + \vec{F}\vec{U}) + \Delta t \frac{\tau}{\rho}\vec{F}\vec{F}\right]}_{\vec{F}_{\text{extra}}}. \tag{24b}$$

One can see that the additional nonlinear terms recovered from the EDM scheme (i.e., $\vec{F}_{\text{extra}}$) are similar to those in the Shan-Chen scheme and both schemes are identical in the case of $\tau = \Delta t$.

6. The LBL scheme

Recently, Lycett-Brown and Luo [42] extended the third-order truncation error analysis and presented a general force implementation scheme which works better under certain circumstances. In this scheme, the discrete form of the force (without considering extra terms to control surface tension) is written as:

$$S_i = w_i\left\{\left[\frac{(\vec{e}_i-\vec{u})}{c_s^2}+\frac{(\vec{e}_i\cdot\vec{u})}{c_s^4}\vec{e}_i\right]\cdot\vec{F}+\gamma\left(\frac{(\vec{e}_i\cdot\vec{F})^2}{2c_s^4\rho}-\frac{\vec{F}\cdot\vec{F}}{2c_s^2\rho}\right)\right\}, \tag{25}$$

where γ is a function of the relaxation time and is defined as follows to achieve exact thermodynamic consistency:

$$\gamma(\tau) = 1-\frac{1}{4\tau}-\frac{\rho}{4Gc_s^2\psi^2\tau}. \tag{26}$$

In this scheme, $\vec{u}^{\text{eq}}=\vec{u}=\sum\vec{e}_i f_i/\rho$ and the macroscopic velocity is calculated by means of Eq. (15). The macroscopic equations corresponding to this method are:

$$\frac{\partial\rho}{\partial t}+\nabla\cdot(\rho\vec{U})=0 \tag{27a}$$

$$\frac{\partial}{\partial t}(\rho\vec{U})+\nabla\cdot(\rho\vec{U}\vec{U}) = -\nabla p+\nu\nabla\cdot[\rho(\nabla\vec{U}+(\nabla\vec{U})^T)]+\vec{F} + \underbrace{\nabla\cdot\left[\left(\tau-\frac{1}{4}-\tau\gamma\right)\frac{\vec{F}\vec{F}}{\rho}\right]+\nabla\cdot\left[\frac{c_s^2}{12}\left[(\nabla\cdot\vec{F})\vec{I}+\nabla\vec{F}+(\nabla\vec{F})^T\right]\right]}_{\vec{F}_{\text{extra}}}. \tag{27b}$$

This scheme reduces to the EDM and the Guo schemes by choosing $\gamma=1$ and $\gamma=1-1/(4\tau)$, respectively. In the above described schemes, the term $\vec{F}_{\text{extra}}$ again is an additional force added to the NS equations.

Generally, in order to match the present schemes to the NS equations, the external force must be small, while the temporal and spatial changes of the external force should be constant or vary slightly. However, $\vec{F}_{\text{extra}}$ may have a great impact on the solution due to the velocity gradient. Huang *et al.* [24] found that the term $\rho^{-1}\vec{F}\vec{F}$ in $\vec{F}_{\text{extra}}$ has negligible effect when simulating single-phase flows. However, this term has a substantial effect on the simulation of multiphase systems and is capable of enhancing numerical stability. In brief, Different forcing schemes, which have different additional terms, may lead to different pressure tensors in the PP-LBM and, consequently, the corresponding solution may differ. For more details see Ref. [25].

D. Incorporating EOS

In this work, three of the most popular EOSs for nonideal flows are considered, viz. the van der Waals (vdW), the Redlich-Kwong (RK), and the Carnahan-Starling (CS) EOS. These EOSs are defined as:

$$\text{vdW}: p_{\text{vdW}}=\frac{\rho RT}{1-b\rho}-a\rho^2, \tag{28a}$$

$$\text{RK}: p_{\text{RK}}=\frac{\rho RT}{1-b\rho}-\frac{a\rho^2}{\sqrt{T}(1+b\rho)}, \tag{28b}$$

$$\text{CS}: p_{\text{CS}}=\rho RT\frac{1+b\rho/4+(b\rho/4)^2-(b\rho/4)^3}{(1-b\rho/4)^3}-a\rho^2, \tag{28c}$$

where a and b are attraction and repulsion parameters, respectively. To incorporate these into the PP-LBM, the selected EOS is substituted into Eq. (10). All three EOSs are two-parameter cubic EOSs. The RK EOS modifies the attraction term of the vdW EOS, whereas the CS modifies the hard sphere term of the vdW EOS [18]. Each EOS has a different performance in terms of thermodynamic inconsistency, density ratio, spurious velocities, and temperature range [18,19,24].

At the critical point, the two phases of a substance become identical. At this point, only one phase exists and the mathematical conditions $[\partial p_{\text{cr}}/\partial V_{\text{cr}}]_{T;\text{cr}}=[\partial^2 p_{\text{cr}}/\partial V_{\text{cr}}^2]_{T;\text{cr}}=0$ should be satisfied. Thus:

$$\text{vdW}: a=0.4218R^2T_{\text{cr}}^2/p_{\text{cr}},\quad b=0.125RT_{\text{cr}}/p_{\text{cr}}, \tag{29a}$$

$$\text{RK}: a=0.4275R^2T_{\text{cr}}^{2.5}/p_{\text{cr}},\quad b=0.0867RT_{\text{cr}}/p_{\text{cr}}, \tag{29b}$$

$$\text{CS}: a=0.4963R^2T_{\text{cr}}^2/p_{\text{cr}},\quad b=0.1873RT_{\text{cr}}/p_{\text{cr}}. \tag{29c}$$

In this work, we set $R=1$ for the simulations, $a=9/49$, $b=2/21$ for the vdW EOS and $a=2/49$, $b=2/21$ for the RK EOS, whereas we set $a=1$ and $b=4$ for the CS EOS. Therefore, the critical temperature and the density for the vdW, the RK, and the CS EOSs are equal to: $T_{\text{cr,vdW}}=4/7$, $\rho_{\text{cr,vdW}}=7/2$; $T_{\text{cr,RK}}=0.1961$, $\rho_{\text{cr,RK}}=2.73$; and $T_{\text{cr,CS}}=0.09432$, $\rho_{\text{cr,CS}}=0.11911$, respectively.

It is worthwhile mentioning that the parameters a, b, and R in the selected EOSs may affect the numerical stability by changing the interface thickness. Huang *et al.* [24] showed that for the CS EOS the value of R has no effect on the interface thickness and numerical stability of the model. By decreasing the attraction parameter, a, the interface width increases [42]. In addition, the densities of the phases are affected by the parameter b, but the density ratio remains constant. Huang *et al.* [24] concluded that $a=1$ and $b=4$ are proper choices to have stable simulations with an optimum interface thickness.

The vdW EOS is an improvement over the ideal gas law and is valid above the critical temperature for a wide range of pressures and temperatures. Below the critical temperature, the equation is qualitatively reasonable for the liquid state and the low-pressure gaseous state [43]. The main advantages of the RK EOS is that not much information is required about the substance or the components of a mixture. Its main drawback is that is not suitable for liquid phase systems or vapor-liquid equilibria but just for gases. The RK EOSs can be used for mixtures and for predicting vapor and liquid properties by applying mixing rules to the equation of state parameters [44]. The CS EOS exhibits a better agreement with experimental data on coexistence curves than the vdW and the RK EOSs and is one of the best analytical EOSs describing the behavior of the rigid-spheres model accurately [19,45].

III. RESULTS AND DISCUSSIONS

In this section, the effects of the various formulations of the potential term on the accuracy and stability of the simulations are analyzed. The main aim of the analyses is to find out how to simulate a (non-)isothermal two-phase system with a high density ratio at low temperature in spite of the presence of spurious velocities. At first, the heat transfer through a flat interface is examined, where there are no spurious velocities. Then the numerical results for a two-dimensional stationary droplet are presented and the effects of spurious velocities on the temperature field around a (non-)isothermal droplet are shown. Furthermore, for the selected potential terms, the effects of different aspects such as EOS, force implementation scheme, viscosity, etc., on the results are studied. Finally, simulation results with optimized parameters for a high density ratio droplet are presented.

In this paper, all quantities are in lattice units. For all case studies, the mesh size is 150 × 150. The thermal diffusivities and specific heats of the liquid and the vapor are set as $\alpha^{\mathrm{liq}} = 0.01$, $\alpha^{\mathrm{vap}} = 0.1$, $c_p^{\mathrm{liq}} = 2.62$, and $c_p^{\mathrm{vap}} = 2.50$, unless stated otherwise. The thermal conductivity k then follows from $k = \rho c_p \alpha$. The reduced temperature and density are defined as $T_r = T/T_{\mathrm{cr}}$ and $\rho_r = \rho/\rho_{\mathrm{cr}}$, respectively. At the liquid-vapor interface, thermohydrodynamics properties η (such as thermal conductivity or specific heat) are calculated by an interpolation scheme as [38]:

$$\eta = \frac{\rho^{\mathrm{liq}} - \rho}{\rho^{\mathrm{liq}} - \rho^{\mathrm{vap}}}\eta^{\mathrm{vap}} + \frac{\rho - \rho^{\mathrm{vap}}}{\rho^{\mathrm{liq}} - \rho^{\mathrm{vap}}}\eta^{\mathrm{liq}}. \tag{30}$$

By using the above definition, the properties changes monotonically within the interface region.

A. Heat transfer through a flat interface

Here an isothermal and a nonisothermal stationary flat vapor-liquid interface are simulated to ensure that the model is capable of simulating correct thermal behavior. The domain is initialized with liquid and vapor phases in the bottom part and top part of the domain, respectively. The Shan-Chen potential term [Eq. (7)] and the Guo implementation scheme [41] are used to calculate the phase separation for $\tau = 1$. Also, it is assumed that the fluid is following the vdW EOS.

For the case of the isothermal system, the temperature of the domain is initialized at $T_r = 0.8$ in the whole domain. For the case of the nonisothermal system, the top and bottom boundaries are considered as constant temperature boundaries and periodic boundary conditions are applied to the lateral boundaries. In this case, the temperature of the top boundary (in contact with the vapor phase) and the bottom boundary (in contact with liquid phase) are set equal to $T_r = 0.8$ and $T_r = 0.7$, respectively [46,47]. For this case, the thermal diffusivities of the liquid and the vapor are set as $\alpha^{\mathrm{liq}} = \alpha^{\mathrm{vap}} = 0.1$. By starting the simulation, heat is transported from the hotter boundary to the cooler boundary, across the interface.

Figure 1(a) shows the density contour plot in the steady-state isothermal condition. The thickness of flat interface is four lattice units and its location is established at $x^* = 0.53$ where x^* is the nondimensionalized spatial coordinate. According to Fig. 1(a) the predicted density ratio is around 11, which is in agreement with the theoretical value at $T_r = 0.8$ based on the coexistence curve of vdW EOS. The temperature profiles along the vertical centerline of the domain for both isothermal and nonisothermal cases are shown in Fig. 1(b). One can see that the temperature remains constant for the case of an isothermal system, while for the nonisothermal system the temperature decreases from the hotter wall toward the cooler wall. Due to the different properties (i.e., ρ and α) of the phases, the temperature gradient changes at the interface. For this case, the thermal conductivities of the liquid and the vapor phases are equal to 1.77 and 0.152, respectively. The numerical temperature profile for the nonisothermal case agrees well with the analytical solution.

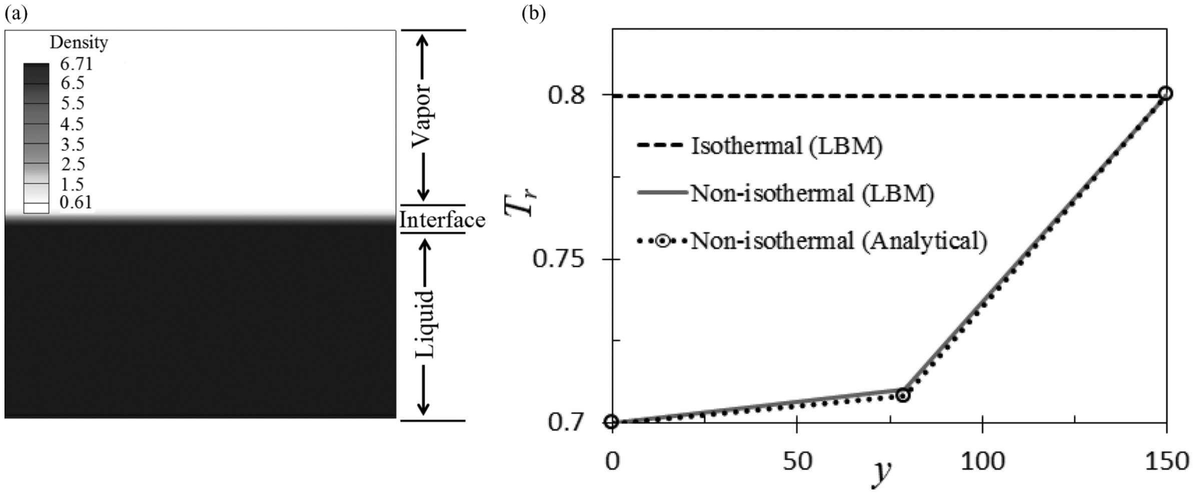

FIG. 1. A two-phase system with a flat interface obeying the vdW EOS: (a) density contour plot at $T_r = 0.8$ and (b) temperature profiles for isothermal and nonisothermal systems.

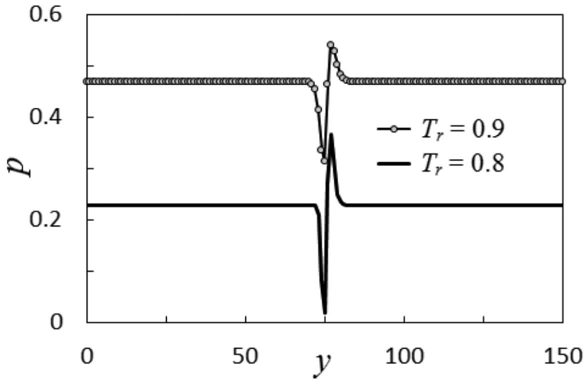

FIG. 2. Pressure distribution throughout the flat interface for a vdW fluid at $T_r = 0.9$ and 0.8.

Figure 2 shows the pressure distribution throughout the flat interface when system obeying the vdW EOS. As we can see the bulk pressures of the liquid and vapor phases are equal. Physically, these results are consistent and reflect the fact that under equilibrium conditions the Gibbs free energy should have the same values in both phases in equilibrium [48]. However, there are variations of the pressure across the interface, which are inconsistent with real life. It indicates that the mechanical stability condition is not satisfied around the interface [24].

Wagner [49] explained that why the lattice Boltzmann methods using a force to introduce the nonideal EOS fails to provide correct prediction for the thermodynamic properties such as pressure around the interface. In the LBM, the macroscopic NS equations are recovered by using the second-order expansion of the lattice Boltzmann equation. A difficult situation occurs when the LBM is used for simulating strongly inhomogeneous fluid composition such as near to an interface. In this case, higher-order density derivatives appear in the NS equations which are non-negligible and are responsible for obtaining a true equilibrium solution. However, these terms are neglected by using a second-order expansion on the lattice Boltzmann equation. Various attempts have been made to overcome this problem. For more details we refer the reader to Refs. [49–51].

B. (Non-)Isothermal stationary droplet

In this section, the effect of spurious velocities on the temperature field is investigated. The test case is a two-phase system in a square domain where a stationary circular droplet with radius $r = 30$ is suspended in its vapor. The simulations are done in a fully periodic domain. Similarly to Sec. IIIA, the simulations are performed for isothermal and nonisothermal conditions. All necessary assumptions and parameters are the same as those used in the previous section for the flat interface, i.e., for the nonisothermal case, and the temperature of the top (hot) wall is set to $T_r = 0.8$, where the temperature of the bottom (cold) wall is equal to $T_r = 0.7$. Initially, the droplet is located at the center of the domain, and after a number of iterations, a steady state is reached.

The density contour plot of the stationary droplet at $T_r = 0.8$ is shown in Fig. 3(a). It is apparent that the density ratio is around 10.5, and the thickness of the interface is 4 in lattice units. The velocity vectors at steady state are shown in Fig. 3(b). It is clear that eight recirculation regions are formed around the interface and they are primarily located in the low-density (vapor) region. The temperature contour plots for the isothermal and the nonisothermal condition at steady state are shown in Figs. 4(a) and 4(b). The results show that, due to the existence of the spurious velocities, four symmetric hot and cold spots are formed around the interface. The temperature profiles along the vertical centerline of the domain for both isothermal and nonisothermal cases are shown in Fig. 5, compared with the analytical solution. The humps in temperature profile are due to the unphysical hot spots and result in deviations from the true physical behavior.

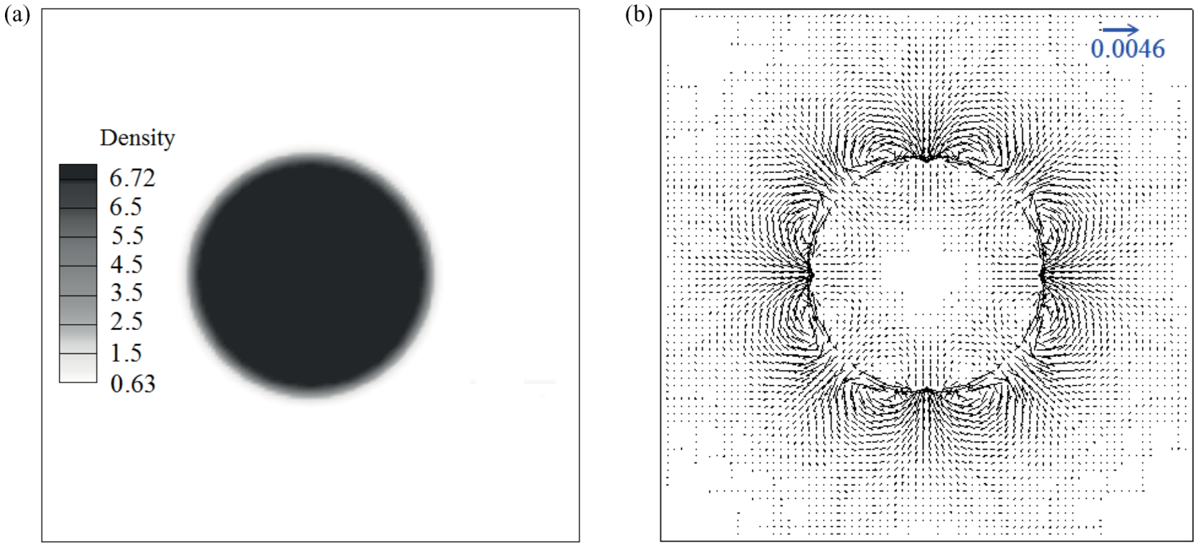

FIG. 3. (Color online) Simulation of the liquid droplet in the vapor obeying the vdW EOS at $T_r = 0.8$: (a) density contour plot and (b) velocity vectors with maximum value equal to 0.0046.

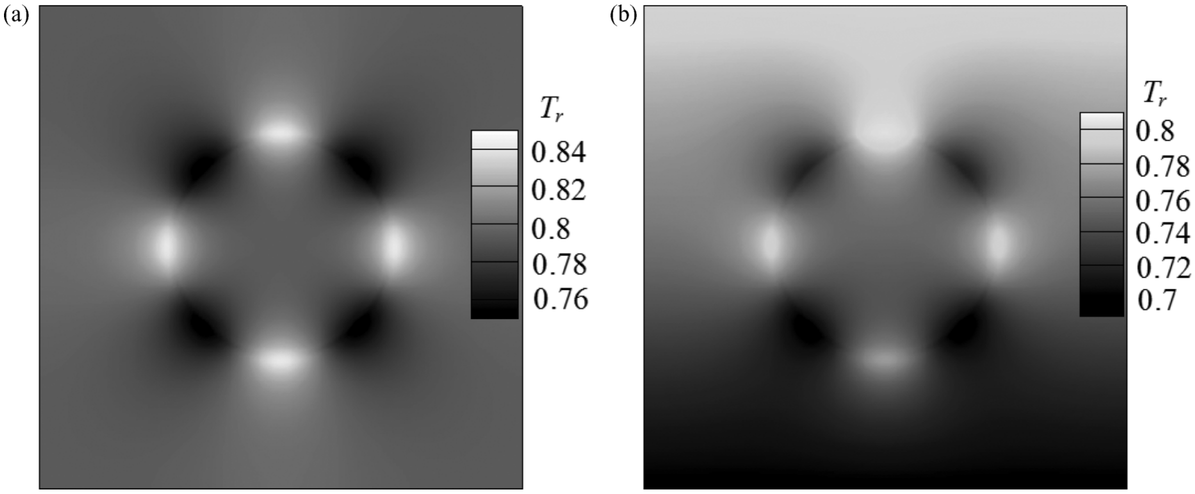

FIG. 4. Temperature contour plots for (a) an isothermal system at $T_r = 0.8$ and (b) a nonisothermal system with $T_{r,\mathrm{hot}} = 0.8$ and $T_{r,\mathrm{cold}} = 0.7$.

C. Assessment of the Shan-Chen potential term

In this section, the performance and the accuracy of the Shan-Chen potential [Eq. (7)] on the thermohydrodynamic behavior of an isothermal stationary droplet with a high density ratio are assessed. Also, the effects of EOS, force implementation scheme, and viscosity (relaxation time) on the simulation results are analyzed and discussed. By selecting proper parameters, the undesirable effects on the numerical artifacts can be reduced, which, consequently, enables stable simulations for a wide range of density ratios.

1. The effect of the EOS

In this part, we compare the simulation results of three EOSs, i.e., vdW, RK, and CS, for an isothermal stationary droplet at different temperatures (or density ratios). The Guo force implementation scheme [38] is used to calculate the fluid flow for $\tau = 1$. In Table I, we compare the maximum value of the spurious velocities ($u_{\max}$) and also the maximum and minimum values of the temperature in the hot and cold spots around the interface. We can see that at all selected reduced temperatures, the values of $u_{\max}$ for the CS EOS are much smaller than the vdW EOS and the RK EOS. Also, it is clear that the rate of increase in spurious velocities with temperature for the RK EOS is much higher than the rates for the other EOSs. All simulations become unstable for $T_r < 0.76$ due to a limitation in the Guo scheme which is discussed in greater details in the next section.

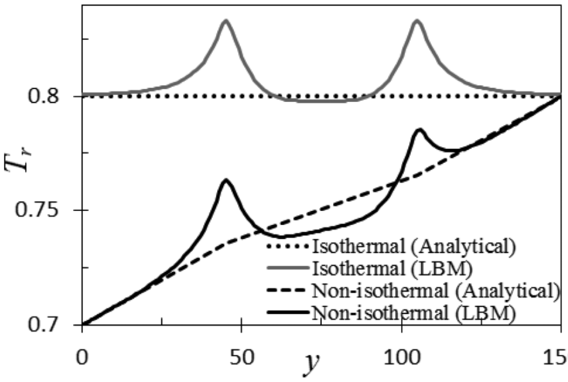

FIG. 5. Temperature profile along the vertical centerline for isothermal system obeying the vdW EOS at $T_r = 0.8$ and nonisothermal system with $T_{r,\mathrm{hot}} = 0.8$ and $T_{r,\mathrm{cold}} = 0.7$.

Figure 6 shows a comparison between temperature profile along the vertical centerline of domain for different EOS at $T_r = 0.85$. We can see that the unphysical temperature humps are virtually absent at $T_r > 0.85$ when using the CS EOS. Obviously, the RK EOS and the vdW EOS have good performance only at high temperatures (or at low density ratios) while the CS EOS performs better for a wide ranges of density ratios than the other two EOSs, due to the small spurious velocities.

To study the effect of the EOSs in some greater detail, simulations are also carried out for $T_r = 0.8$ and 0.7 by using the EDM implementation scheme. For $T_r = 0.8$ we found that the interface thicknesses are approximately 5, 6, and 10 in lattice units for the RK, the vdW, and the CS EOSs, respectively, while for $T_r = 0.7$ the thicknesses are 4, 5, and 9 for the RK, the vdW, and the CS EOSs, respectively. We found that by decreasing the temperature, the interface thickness decreases and for lower temperatures when the interface thickness is just 3, the simulations become unstable. Also, the CS EOS leads to a thicker interface in comparison with the other EOSs. In general, the interface width had a great effect on the stability of the model. The EOS affects the interface thickness and, consequently, the stability of the simulations. The results show that, by decreasing the temperature (or increasing the density ratio), the simulations with the RK EOS become unstable sooner than the vdW EOS, which in turn becomes unstable sooner than the CS EOS. Therefore, the CS EOS is used for the rest of the simulations.

2. The effect of the force implementation scheme

In this section, the effect of six different forcing schemes, i.e., the Shan-Chen scheme [12], the He scheme [39], the BG scheme [40], the Guo scheme [41], the EDM [19], and the LBL scheme [42], on the numerical results of the isothermal stationary droplet is discussed. Coexistence curves of the CS EOS for different relaxation times are presented in Fig. 7.

TABLE I. Maximum spurious velocities and maximum/minimum temperature obtained from simulation of isothermal stationary droplet for different EOSs using the Shan-Chen potential term and the Guo force implementation scheme [41].

	RK EOS			vdW EOS			CS EOS		
T_r	$u_{\max}$	T_{hot}	T_{cold}	$u_{\max}$	T_{hot}	T_{cold}	$u_{\max}$	T_{hot}	T_{cold}
0.9	0.002176	0.9171	0.8786	0.001053	0.9035	0.8954	0.000122	0.9003	0.8993
0.85	0.005069	0.9231	0.7761	0.002519	0.8647	0.8299	0.000287	0.8516	0.8487
0.8	0.022574	1.2094	0.6731	0.004624	0.8325	0.7621	0.000577	0.8088	0.7917
0.77	N/A	N/A	N/A	0.006251	0.8488	0.6975	0.002196	0.7924	0.7523

Numerical results for the Shan-Chen force implementation scheme [Fig. 7(a)] show a good agreement with the analytical solution when $\tau = 1$ and $T_r \geqslant 0.75$. However, as the temperature is reduced (i.e., smaller than 0.75), the simulation results begin to deviate from the analytical solution and, finally, diverges for $T_r < 0.55$. Also, the scheme remains stable for $\tau > 1$ until low reduced temperatures ($T_r < 0.35$), whereas the solution is unstable at $\tau = 0.8$ for $T_r < 0.75$. We can see that the results of the Shan-Chen force implementation are quite dependent on the relaxation time.

The results for the He [39] and the BG [40] schemes are presented in Figs. 7(b) and 7(c) respectively. It is clear that these schemes are stable for a narrow range of temperatures only (i.e., $T_r \geqslant 0.85$ for the He [39] scheme and $T_r \geqslant 0.82$ for the BG [40] scheme). However, these schemes are almost independent of the relaxation time and agree well with the analytical solution when $T_r \geqslant 0.88$. The numerical results for the Guo scheme [Fig. 7(d)] show that this scheme is independent of relaxation time and yields satisfactory results for $T_r \geqslant 0.85$. However, the scheme becomes unstable at $T_r < 0.76$ for $\tau = 1$ and at $T_r < 0.79$ for $\tau = 0.8$ and 1.2. We conclude that the He [39], the BG [40], and the Guo [41] schemes are applicable for low density ratio (less than 35). Thus, since we aim to simulate the problem at high density ratios, these schemes are not a proper choice and are not discussed further.

As shown in Fig. 7(e), the EDM scheme gives satisfactory and stable results for a wide range of reduced temperatures, irrespective of the relaxation time used. The simulation results deviate from the analytical solution for $T_r < 0.75$ and, finally, become unstable at $T_r = 0.55$. Comparing the results of the Shan-Chen and the EDM schemes for $\tau = 1$, we can see that the results are the same, which is in accordance with the discussion presented in Sec. IIC. Figure 7(f) shows the coexistence curve obtained by use of the LBL scheme [42] compared with the analytical solution. The results indicate that the scheme is independent of the relaxation time and remains stable until low temperatures. However, the vapor density is always overestimated. The general impression is that the EDM and the LBL implementation schemes perform best in terms of the density ratio.

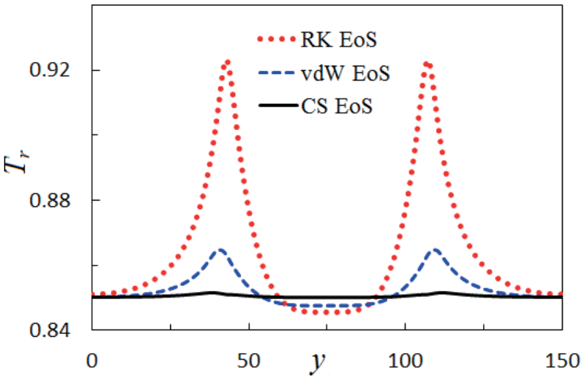

FIG. 6. (Color online) Temperature profile along the vertical centerline for isothermal system at $T_r = 0.85$ for different EOSs.

The magnitude of the total force term and the distribution of the extra force terms in the EDM [19] and the LBL schemes [38] along the vertical centerline of the domain at $T_r = 0.8$ are shown in Fig. 8(a). At this temperature, the total forces calculated by these schemes almost exclusively differ due to the extra force term [see Eqs. (24b) and (27b)]. It is clear that the total force peaks at the interface and tends to zero in the bulk regions. Also, the extra force terms only affect the interface region and are small compared to the total force. The plots of the extra force term for $T_r = 0.9$ and 0.8 for the EDM scheme are shown in Fig. 8(b). As the reduced temperature decreases, the density ratio and, consequently, the total force and the spurious velocities grow (see Sec. IIIC3) which in turn result in an increase of the extra force term.

3. *The effect of relaxation time*

In this section, the effect of the relaxation time (or viscosity) on the simulation results is discussed. Table II illustrates the resulting equilibrium density ratio ($\rho^* = \rho^{\text{liq}}/\rho^{\text{vap}}$) as found in our simulations for the Shan-Chen [12], the EDM [19], and the LBL [42] force implementation schemes at different reduced temperatures for $\tau = 0.8$, 1, and 1.2. The data show that the EDM scheme performs better than the Shan-Chen scheme when $\tau < 1$, whereas the Shan-Chen scheme is more stable when $\tau > 1$. The Shan-Chen scheme depends on the value of τ, which is undesirable, whereas the EDM scheme is independent of relaxation time for a wide range of T_r. However, the EDM scheme is sensitive to the relaxation time at low reduced temperatures. The predicted density ratio as a function of relaxation time using the EDM scheme is shown in Fig. 9. The density ratio starts varying with relaxation time for $T_r < 0.7$. It is clear that the deviation of the predicted density ratio from the analytical value is higher at low relaxation times, which is due to the effect of the coefficient of the term $\nabla \cdot [\rho^{-1}\vec{F}\vec{F}]$, which is τ^2 and $\tau\Delta t$ for the Shan-Chen and the EDM schemes, respectively. Our results are in agreement with the data presented in Ref. [24] for high temperatures. By decreasing the temperature to values lower than 0.7, the effect

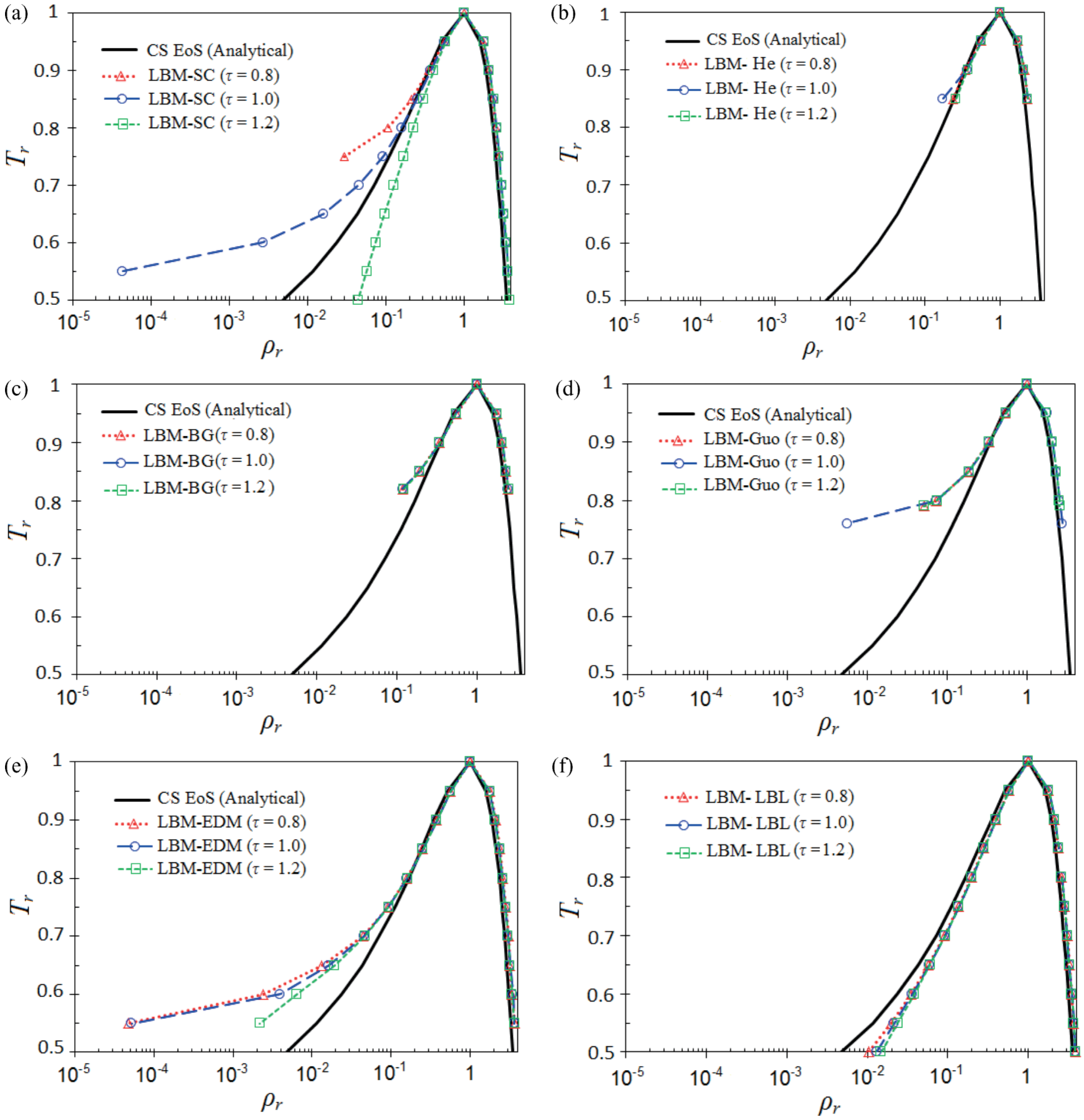

FIG. 7. (Color online) Comparison between the analytical coexistence curve of the CS EOS and the LBM simulation results for $\tau = 0.8$, 1, and 1.2 using (a) the Shan-Chen [12], (b) the He [39], (c) the BG [40], (d) the Guo [41], (e) the EDM [19], and (f) the LBL [42] force implementation schemes.

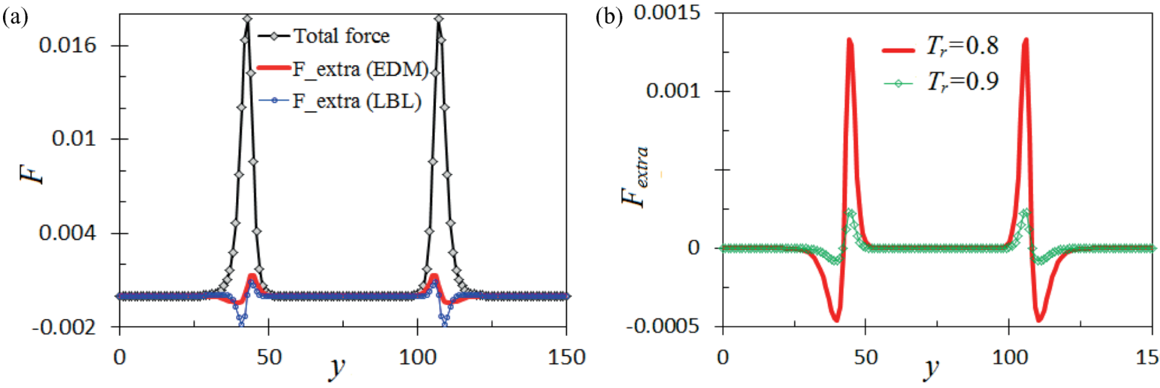

FIG. 8. (Color online) (a) Distributions of the total force and the extra force term for the EDM [19] and the LBL [42] schemes at $T_r = 0.8$ and $\tau = 1$, (b) extra force distributions of the EDM scheme for $T_r = 0.9$ and 0.8. Results are with reference to the CS EOS.

TABLE II. Equilibrium density ratio obtained from the Shan-Chen [12], the EDM [19], and the LBL [42] force implementation schemes at different reduced temperatures for $\tau = 0.8$, 1, and 1.2. (Note: N/A means not applicable and the simulation becomes unstable at this temperature.)

	CS EOS	$\tau = 0.8$			$\tau = 1$			$\tau = 1.2$		
T_r	ρ^*_{Exact}	$\rho^*_{\text{Shan-Chen}}$	ρ^*_{EDM}	ρ^*_{LBL}	$\rho^*_{\text{Shan-Chen}}$	ρ^*_{EDM}	ρ^*_{LBL}	$\rho^*_{\text{Shan-Chen}}$	ρ^*_{EDM}	ρ^*_{LBL}
0.95	3.1	3.2	3.2	3.1	3.1	3.1	3.1	3.1	3.1	3.1
0.9	5.5	5.9	5.5	5.3	5.5	5.5	5.3	5.1	5.5	5.3
0.85	8.8	10.9	9.4	8.4	9.3	9.3	8.4	7.9	9.3	8.4
0.8	14.1	24.4	16.3	13.1	16.4	16.6	13.1	11.5	16.1	13.1
0.75	22.9	94.3	30.6	20.7	30.2	30.2	20.6	16.6	30.9	20.5
0.7	38.5	N/A	69.3	33.4	66.8	66.8	33.1	23.6	64.1	32.7
0.65	68.4	N/A	242.8	56.1	197.1	197.4	54.8	33.1	166.2	53.4
0.6	131.9	N/A	1428.4	98.1	878.9	878.7	93.9	46.2	531.2	88.9

of the relaxation time on the predicted density ratio becomes more pronounced. The results for the LBL scheme in Table II indicate that the performance of this scheme does not improve upon increasing the relaxation time. As a result, this scheme predicts the density ratio with a good accuracy for a wide range of temperature (i.e., $T_r \geqslant 0.7$). However, the results become sensitive to the relaxation time at lower temperatures which is due to the coefficient $(\tau - 1/4 - \tau\gamma)$ of the term $\nabla \cdot [\rho^{-1}\vec{F}\vec{F}]$ in Eq. (27b).

The maximum value of the spurious velocities as well as the maximum/minimum values of temperature in the isothermal domain using the Shan-Chen [12], the EDM [19], and the LBL [42] force implementation schemes are presented in Tables III and IV for $\tau = 0.8$ and 1.2, respectively. From the results, we find that there are no significant differences in the spurious velocities and the maximum and minimum temperatures between all the force implementation schemes at $T_r > 0.7$ for any τ. At lower temperatures, however, the LBL scheme performs better than the EDM scheme. The results show that by increasing the relaxation time, the magnitude of the spurious velocities increases for all schemes. For $\tau = 1.2$ and $T_r < 0.7$, the maximum spurious velocities and, consequently, the deviation of the temperature from the isothermal condition for the EDM scheme are greater than with the Shan-Chen and the LBL schemes. The performance of the Shan-Chen scheme and the LBL scheme are almost the same for $\tau = 1.2$ for the temperatures chosen.

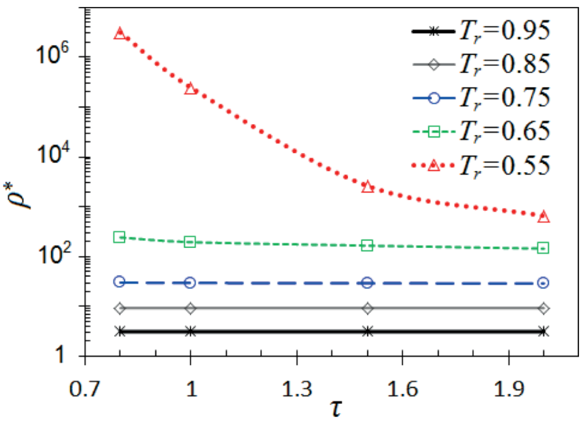

FIG. 9. (Color online) Comparison of the predicted density ratio using the EDM scheme [19] vs relaxation time at different temperatures with reference to the CS EOS.

In addition to the relaxation time, the density ratio and the temperature are other important issues, which affect the simulation results. From the coexistences curve of the EOS (see Fig. 7 and Table II), we can see that the density ratio increases as the temperature decreases. The overall effect is higher spurious velocities and, consequently, more serious unphysical behavior in the temperature domain (see Tables III and IV). Therefore, by decreasing the temperature, the density ratio increases and the spurious velocities may become high enough to turn the simulation unstable.

Figure 10 shows the comparison of the achievable lowest temperature according to the selected force implementation schemes as function of the relaxation time. Mostly, by increasing the relaxation time, the achievable lowest temperature decreases. The achievable lowest temperature defines as the lower limit of the temperature, at which the simulation remains stable. The reason is that by decreasing the relaxation time, the collision operator becomes larger, which, consequently, leads to less numerical stability. Also, it is clear that the stability of the LBL scheme is better than other schemes for every τ. Furthermore, the numerical stability of the EDM scheme is better than that of the Shan-Chen scheme when $\tau < 1$. As discussed earlier, the EDM and the Shan-Chen schemes are identical at $\tau = 1$. For $\tau > 1$, the Shan-Chen scheme results in slightly lower temperature than the EDM scheme.

According to above analyses, the density ratio and, consequently, the surface tension in the Shan-Chen scheme strongly depend on τ and large differences between the numerical and analytical results are observed for $T_r < 0.85$ as well as $\tau > 0.7$. Therefore, this scheme is not discussed further and the following results will focus on the EDM and the LBL schemes.

Figure 11(a) shows the maximum value of the spurious velocities in the isothermal domain as a function of relaxation time using the EDM and the LBL schemes for $T_r = 0.75$ and 0.65. It is clear that the spurious velocities increase when the relaxation time is increased. Also, there is no significant difference between the maximum values of the spurious velocities when using the EDM or the LBL schemes. However, as the temperature decreases to values lower than 0.7, the EDM scheme predicts larger spurious velocities due to the deviation from the analytical solution [see Fig. 7(e)].

TABLE III. Maximum spurious velocities and maximum and minimum values of temperature calculated by the Shan-Chen [12], the EDM [19], and the LBL [42] force implementation schemes for $\tau = 0.8$ at different T_r.

	Shan-Chen			EDM			LBL		
T_r	$u_{\max}$	T_{hot}	T_{cold}	$u_{\max}$	T_{hot}	T_{cold}	$u_{\max}$	T_{hot}	T_{cold}
0.95	0.000074	0.9515	0.9484	0.000026	0.9509	0.9491	0.000015	0.9507	0.9499
0.9	0.000082	0.9016	0.8989	0.000081	0.9013	0.8994	0.000079	0.9005	0.8999
0.85	0.000219	0.8525	0.8442	0.000205	0.8522	0.8498	0.000204	0.8512	0.8489
0.8	0.000418	0.8015	0.7926	0.000401	0.8014	0.7952	0.000415	0.8034	0.7966
0.75	0.000889	0.7604	0.7408	0.000611	0.7542	0.7432	0.000708	0.7571	0.7427
0.7	N/A	N/A	N/A	0.001101	0.7128	0.6915	0.001087	0.7115	0.6881
0.65	N/A	N/A	N/A	0.001595	0.6719	0.6415	0.001565	0.6646	0.6335
0.6	N/A	N/A	N/A	0.002153	0.6195	0.5912	0.002102	0.6163	0.5893

The temperature distributions along the vertical centerline of the computational domain for isothermal systems at $T_r = 0.75$ and 0.65 are shown in Figs. 11(b) and 11(c). By increasing the relaxation time, the unphysical temperature humps (i.e., hot and cold spots) become more pronounced. In agreement with the maximum values of the spurious velocities, the LBL scheme is able to damp the hot and cold spots better than the EDM schemes for $T_r < 0.7$.

Figure 12 shows a comparison between the temperature profiles along the vertical centerline of the computational domain when using the EDM and the LBL schemes for different values of τ and $T_r = 0.65$. According to this figure and Tables II and III, the temperature humps are more or less the same for both schemes. Upon further decreasing the temperature, these humps are slightly smaller with the LBL scheme, which is due to the lower predicted density ratio and, consequently, lower spurious velocities in comparison with the EDM scheme.

To finish this section, we conclude that the combination of the Shan-Chen potential term [Eq. (7] with the CS EOS and the EDM [19] or the LBL [42] force implementation scheme leads to quantitatively good results for the simulation of two-phase systems with low density ratios. According to the above analyses, the EDM scheme predicts liquid and vapor densities with high accuracy for $T_r > 0.7$. Also, the scheme behaves independent of the relaxation time for $T_r > 0.7$ (see Fig. 9) and remains stable up to higher density ratios. However, the EDM scheme is not able to control the dependency of the method on the relaxation time and, consequently, the results deviate from the exact solution for $T_r < 0.7$. On the contrary, the LBL scheme is a quite stable scheme up to very high and low density ratios and temperatures and behaves independently of the relaxation time for $T_r \geqslant 0.6$. The density ratio of the multiphase system is predicted very well by using the LBL scheme, although the vapor density is always overestimated and is higher than the theoretical values.

D. Assessment of the β-scheme potential term

All of the previous results are based on the application of the Shan-Chen potential term [Eq. (7)]. In this section, we compare the performance of the potential terms given by the Shan-Chen force term [Eq. (7)] and the β-scheme force term [Eq. (13)] with reference to the CS EOS and the EDM [19] and the LBL [42] schemes as force implementation methods. The β scheme can be tuned by varying the weighting factor β which depends on the selected equation of state (EOS) [23].

As discussed earlier, the vapor density is overestimated by combining the Shan-Chen potential term [Eq. (7)] and the LBL force implementation scheme [39]. In other words, the density ratio, ρ^*, is always smaller than the theoretical one, while the difference, which represents the thermodynamic inconsistency, increases as the temperature decreases. In order to increase the thermodynamic consistency of the model and solve this issue, we propose to use the β-scheme force [Eq. (13)] and combine it with the LBL implementation scheme. Considering the overestimation of the vapor density and lower density ratio compared with the analytical solution,

TABLE IV. Maximum spurious velocities and maximum and minimum values of temperature calculated by the Shan-Chen [12], the EDM [19], and the LBL [42] force implementation schemes for $\tau = 1.2$ at different T_r.

	Shan-Chen			EDM			LBL		
T_r	$u_{\max}$	T_{hot}	T_{cold}	$u_{\max}$	T_{hot}	T_{cold}	$u_{\max}$	T_{hot}	T_{cold}
0.95	0.000039	0.9503	0.9494	0.000032	0.9502	0.9499	0.000034	0.9502	0.9499
0.9	0.000196	0.9012	0.8989	0.000162	0.9012	0.8995	0.000175	0.9009	0.8993
0.85	0.000512	0.8562	0.8445	0.000374	0.8537	0.8466	0.000432	0.8543	0.8461
0.8	0.000706	0.8162	0.7858	0.000727	0.8116	0.7893	0.000838	0.8131	0.7879
0.75	0.001919	0.7852	0.7222	0.001951	0.7795	0.7259	0.001788	0.7808	0.7233
0.7	0.003162	0.7662	0.6528	0.003222	0.7661	0.6542	0.003621	0.7595	0.6531
0.65	0.006002	0.7523	0.5895	0.011002	0.7866	0.6093	0.006842	0.7399	0.5883
0.6	0.008123	0.7324	0.5641	0.013056	0.7935	0.5042	0.012245	0.7299	0.5261

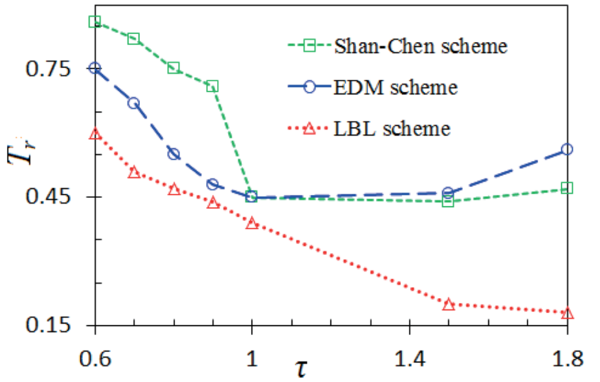

FIG. 10. (Color online) The lowest reduced temperature predicted by the Shan-Chen [12], the EDM [19], and the LBL [42] schemes for different relaxation time with reference to the CS EOS.

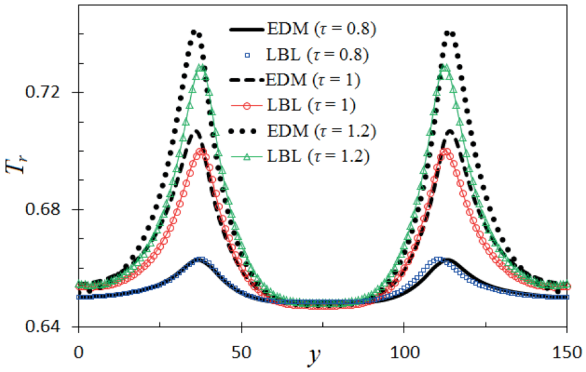

FIG. 12. (Color online) Temperature profile along the vertical centerline of the domain resulted from the EDM [19] and the LBL schemes [42] at different τ for $T_r = 0.65$ with reference to the CS EOS.

we submit the attraction force, $\vec{F}_{\text{potential}}$ to be not strong enough. Therefore, we need to increase the potential force to decrease the vapor density and approach the density ratio to the analytical solution. For this purpose and considering the β-scheme force term [Eq. (13)], we have to choose $\beta < 1$.

Figure 13(a) shows a comparison between the analytical coexistence curves for the CS EOS and numerical data calculated by the β-scheme force term. Here $\tau = 1$ and the LBL scheme is used to include force in the model. The liquid density is calculated with a high accuracy when using both the Shan-Chen and β-scheme force terms. The results for $\beta = 0.9$ in Fig. 13(a) show that also the vapor branch is corrected quite well, but the scheme becomes unstable for $T_r < 0.65$. By slightly increasing the value of β to 0.92 the model remains stable until $T_r = 0.5$, whereas the numerical data have lower accuracy compared with $\beta = 0.9$. In $T_r = 0.5$ the analytical density ratio is 724.7, whereas the numerical density ratio using Shan-Chen force term and the β-scheme force term (with $\beta = 0.92$) is 295.1 and 503.2, respectively. There results show that by using the β scheme the density ratio is improved. However, $\rho^* = 503.2$ is the maximum achievable density ratio in $T_r = 0.5$ using the LBL implementation scheme. The reason is that in order to get a more accurate density ratio we should decrease the value of β, rendering the method less stable, while by increasing the value of β the deviation of ρ^* from the analytical solution increases. We therefore conclude that the LBL scheme is not able to handle high potential forces at low temperatures ($T_r < 0.5$) to achieve an accurate density ratio. This issue might be resolved by adding an additional term to account for higher-order error terms and increasing the interface width by decreasing the attraction coefficient a in the EOS as described in Ref. [42]. After all, the LBL scheme is not able to predict the density ratio accurately in the case of a sharp interface at lower temperatures—not even by combining with the β scheme.

A comparison between the maximum value of the spurious velocities calculated by the Shan-Chen and the β-scheme force terms (with $\beta = 0.92$) is shown in Fig. 13(b). Obviously, there is no significant difference between the values of spurious velocities. The spurious velocities with the β scheme at lower temperatures increase slightly, due to the increase in the density ratio.

In the following, we report the above simulations but now with the EDM scheme for the force implementation. Comparisons between the analytical coexistence curves for CS EOS with numerical data obtained with the Shan-Chen [Eq. (7)] and the β-scheme force terms [Eq. (11)] are shown in Fig. 14(a).

Again, the liquid branch of the coexistence curve is reproduced well using both the Shan-Chen and the β-scheme force terms. As discussed before, the combination of the Shan-Chen force term and the EDM scheme faces problems at the vapor branch and deviates from the theoretical results at low temperatures. This deviation becomes larger as the temperature decreases and, finally, the simulation becomes unstable for $T_r < 0.55$. Since the vapor density is underestimated in this model and the density ratio is higher than the theoretical solution, we choose $\beta > 1$ to decrease the potential force

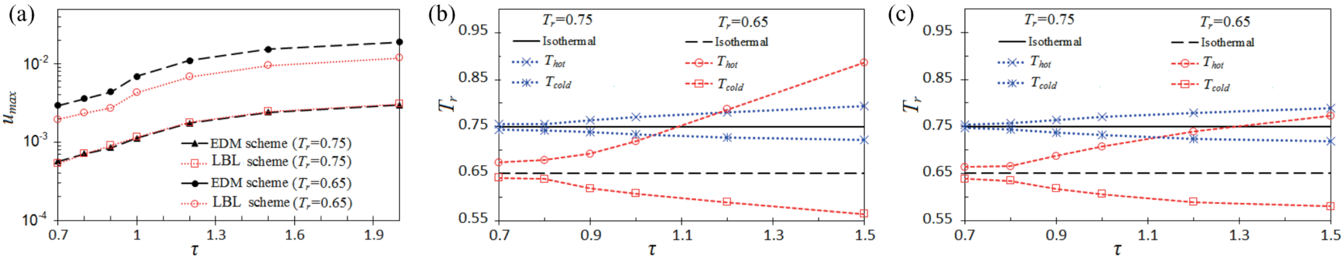

FIG. 11. (Color online) (a) Comparison of spurious velocities for the EDM [19] and the LBL [42] schemes vs relaxation time. Temperature hot and cold spots vs relaxation time in an isothermal system calculated by (b) the EDM scheme and (c) the LBL scheme. All results relate to the CS EOS.

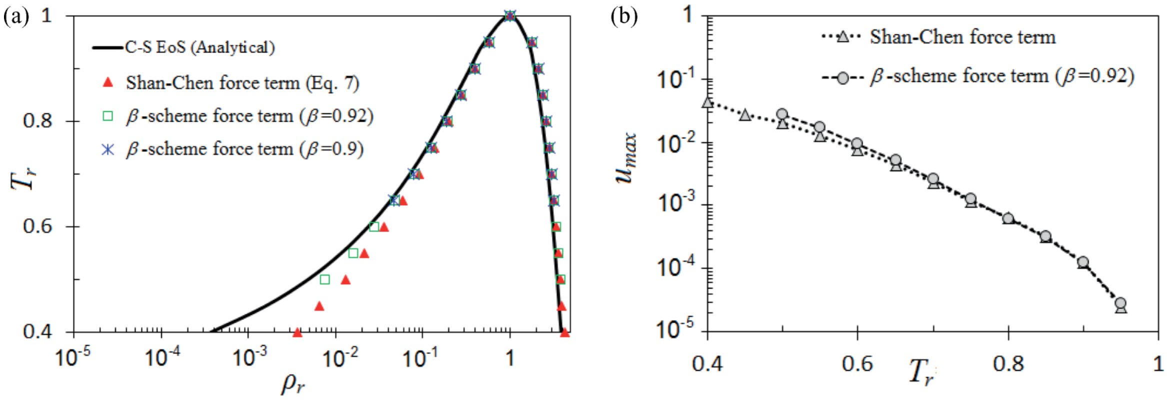

FIG. 13. (Color online) (a) Comparison of the analytical CS EOS coexistence curve and the numerical curves calculated by the Shan-Chen and the β-scheme force terms and (b) comparison of the spurious velocities as function of T_r obtained from the Shan-Chen and the β-scheme terms. Here $\tau = 1$ is used along with the LBL scheme [42] for the force implementation.

[see Eq. (13)] and correct the predicted vapor density. The β scheme with $\beta = 1.25$ gives stable results and coincides with the theoretical results for a wide range of temperatures. The calculated density ratio at $T_r = 0.4$ is equal to 9445, which is within 10% of the analytical density ratio of 10 500. The maximum numerical density ratio is much higher than found in typical real-world applications; even those involving liquid metals [52]. However, it should be noted that this is an upper bound and that this method allows us to reproduce such high density ratios if necessary.

A comparison between the maximum value of the spurious velocities calculated by the Shan-Chen and the β schemes is shown in Fig. 14(b). It is clear that the β-scheme force term gives lower spurious velocities in comparison with the Shan-Chen force term and the increase of the spurious velocities at low temperature is smaller. However, the calculations become unstable for $T_r < 0.39$ only. Based on the above analysis, we use the EDM scheme as the force implementation scheme for the rest of our simulations.

A comparison of the temperature profiles along the vertical centerline of the domain at isothermal condition with $T_r = 0.65$ and 0.7 as computed by the Shan-Chen [Eq. (7)] and the β-scheme [Eq. (13)] terms is shown in Fig. 15. With both forces, the unphysical behavior of the temperature becomes more pronounced upon decreasing the temperature. The unphysical behavior of the temperature decreases in the simulations using the β scheme is less pronounced than when using the Shan-Chen force term, which is due to a decrease in the spurious velocities.

As discussed earlier and as shown in Fig. 9, selecting the EDM scheme as the force implementation scheme renders the density ratio sensitive to the relaxation time for $T_r < 0.7$. Figure 16 shows the predicted density ratio at $T_r = 0.65$ and 0.5 as a function of the relaxation time for different values of β. With the EDM scheme the density ratio changes with relaxation time for any value of β. In itself, this is undesirable behavior which becomes more pronounced upon decreasing the temperature. Small changes in the value of β have a significant effect on the predicted density ratio, especially at low temperatures.

The promising point of this analysis is that at a specific value of the relaxation time, the predicted density ratio coincides exactly with the analytical solution by choosing a proper value for β. Alternatively, we can get rid of the unphysical behavior of the EDM scheme by tuning the value of β such that the exact density ratio is obtained at any relaxation time.

Therefore, in order to achieve the exact density ratio, the value of β cannot be hold constant for an EOS over some

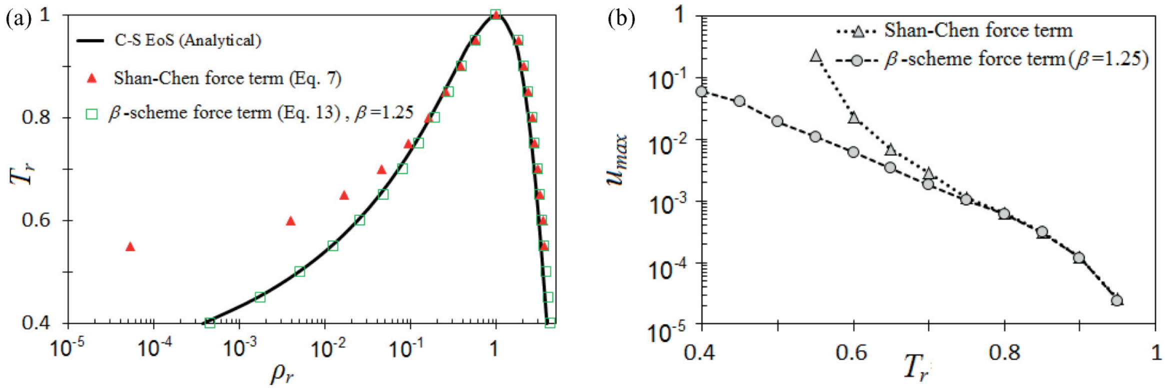

FIG. 14. (Color online) (a) Comparison of the analytical CS EOS coexistence curve and the numerical curves calculated by the Shan-Chen and the β-scheme force terms, (b) comparison of the spurious velocities as function of T_r obtained from the Shan-Chen and the β-scheme terms. Here $\tau = 1$ and the EDM scheme [19] for the force implementation are used.

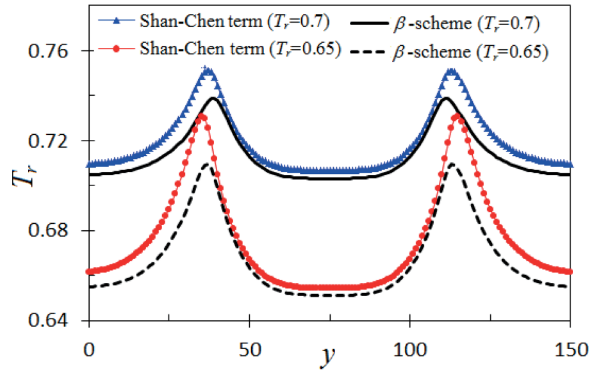

FIG. 15. (Color online) Comparison of the temperature profiles along the vertical centerline of the computational domain for the Shan-Chen and the β-scheme terms for $\tau = 1$, at $T_r = 0.65$ and 0.7.

range of reduced temperatures. As an example, the value of the density ratio based on the CS EOS at $T_r = 0.65$ is 68.4. By setting $\beta = 1.25$ the predicted density ratio equals 68.4 at $\tau = 0.9$ and is equal to 59.5 at $\tau = 2$. But by selecting $\beta = 1.20$ the predicted density ratio is equal to 68.1 at $\tau = 2$. More quantitative comparisons are presented in Table V. In the table, the values of β which result in the correct density ratio are presented for various temperatures at different relaxation times. It is not possible to reach an accurate density ratio for $\tau = 1.5$ or higher, while the maximum density ratio is obtained for $\beta = 1$.

E. Temperature field with suggested parameters

Finally, we implement all of the suggested parameters to capture the temperature field in simulating both an isothermal and a nonisothermal droplet. For this purpose, the CS EOS is adopted as optimum EOS and the EDM and the β-scheme term are implemented as force implementation scheme and potential term, respectively.

In order to evaluate the scheme quantitively, the Laplace tests for droplets of various sizes are carried out. According to the Laplace law, the pressure difference between the inside and outside of the droplet (Δp) over $1/r$ should be a straight line. Figure 17 shows that the results satisfy the linear relation well with the slope equal to the surface tension coefficient σ. The surface tension comes out to be 13.2×10^{-3} and 37.3×10^{-3} for $T_r = 0.8$ and 0.6, respectively. In the equilibrium state at $T_r = 0.8$, cases with radius $r = 49.8$, 39.7, 29.7, and 19.6 result in density ratios $\rho^* = 13.9$, 13.8, 13.7, and 13.4, respectively. Also, the surface tension coefficients are equal to 13.27×10^{-3}, 13.18×10^{-3}, 13.15×10^{-3}, and 13.11×10^{-3}, consequently. The maximum relative density ratio and surface tension differences are less than 3.3% and 3.8%, respectively. A similar story is observed for $T_{r,} = 0.6$.

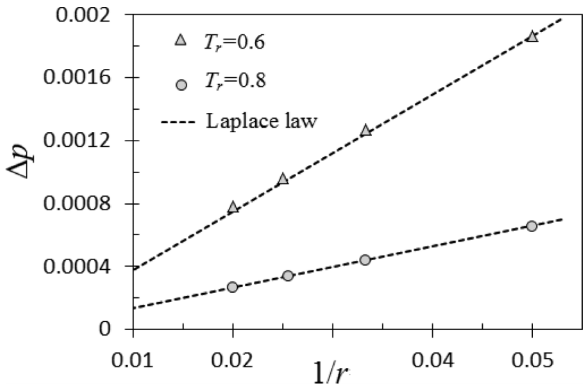

FIG. 17. Comparison of the simulation results at $T_r = 0.8$ and 0.6 with the Laplace law.

Figure 18 shows the temperature profile along the vertical centerline of the computational domain for different isothermal temperatures at $\tau = 0.8$. It is clear that the unphysical effects in the vicinity of the interface are negligible for a wide range of temperatures ($T_r > 0.7$). However, by decreasing the temperature, the unphysical peaks in the temperature domain become more pronounced. This phenomenon becomes significant at high density ratio and low temperature, i.e. $T_r = 0.45$ where the maximum error is about 14%.

The temperature profiles for two nonisothermal cases are plotted in Fig. 19. The result for the case similar to that of Fig. 4 , i.e. $T_{\mathrm{hot}} = 0.8$ and $T_{\mathrm{cold}} = 0.7$, shows that the numerical profile has a very good agreement with the exact solution and there is only a negligible deviation in the vicinity of the interface near the cooler boundary. For high density ratio, i.e., $T_{\mathrm{hot}} = 0.6$ and $T_{\mathrm{cold}} = 0.5$, the deviation from the exact solution becomes more pronounced and is about 10%.

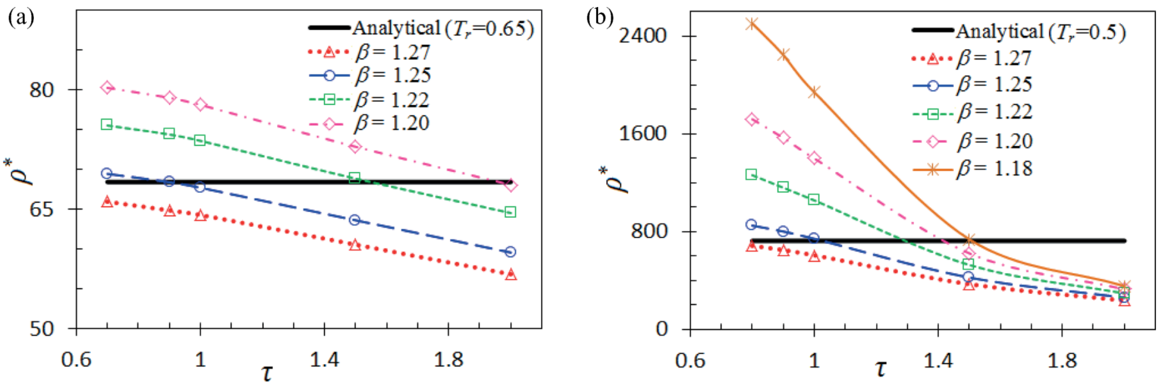

FIG. 16. (Color online) Comparison of the predicted density ratio when using the EDM vs relaxation time for different values of β at (a) $T_r = 0.65$ and (b) $T_r = 0.5$.

TABLE V. The values of β to calculate exact density ratio for various temperatures at different relaxation time.

	$T_r = 0.65$ ($\rho^*_{\text{exact}} = 68.4$)		$T_r = 0.60$ ($\rho^*_{\text{exact}} = 131.9$)		$T_r = 0.50$ ($\rho^*_{\text{exact}} = 724.7$)		$T_r = 0.45$ ($\rho^*_{\text{exact}} = 2328.1$)	
τ	β	ρ^*	β	ρ^*	β	ρ^*	β	ρ^*
0.8	1.25	68.4	1.259	132.8	1.264	726.3	1.265	2334.3
1	1.24	69.6	1.249	132.9	1.252	727.6	1.251	2314.4
1.5	1.22	68.8	1.213	131.4	1.188	721.9	1.000	1055.2

IV. CONCLUSIONS

The PP-LBM was used to simulate single-component isothermal and nonisothermal multiphase systems with a high density ratio. In order to include the effect of spurious velocities, a two-dimensional droplet was considered as a case study. In this work, some important issues about two most common interaction potential terms, namely the Shan-Chen and the β-scheme terms were studied. It was found that the Shan-Chen potential term predicts good results for multiphase systems with low a density ratios (i.e.,53 high temperature: $T_r > 0.7$) cases if it is combined with the CS EOS and the EDM or the LBL force implementation schemes. However, this scheme was not able to control the dependency of the model on relaxation time and, consequently, the results deviate from the exact solution for $T_r < 0.7$. The studies showed that the EDM force implementation scheme and also the CS EOS have significant effects on the magnitude of the spurious velocities and thereby on the stability of the simulations. Also, the combination of the LBL scheme and the Shan-Chen force term leads to quantitatively good results for the simulation of two-phase systems with low density ratios. In fact, the LBL scheme is a quite stable scheme up to very high density ratios and behaves independent of the relaxation time for $T_r \geqslant 0.6$. The density ratio of the multiphase system is predicted very well by using the LBL scheme, however, the vapor density is always overestimated and is higher than the theoretical values.

By selecting the β scheme force term as the interaction potential term in the model, we could reach to high density ratios (or low temperatures) for multiphase systems in spite of the presence of spurious velocities. We showed that by choosing a proper values for β, the results of the LBL scheme improve and the vapor density is corrected. However, the solution was limited to higher and lower temperatures and density ratios. Furthermore, it was not possible to achieve an accurate density ratio at low temperatures ($T_r < 0.5$) by using the LBL scheme and the density ratio was lower than the accurate solution.

By combining the β-scheme force term and the EDM scheme we were able to reduce the dependency of the force implementation on the relaxation time. Thus, we could diminish the undesirable dependency of the EDM scheme on the relaxation time (for low temperatures) by tuning the value of β and reach to the exact density ratio at any relaxation time. The β scheme helps to improve the stability of the simulations and to decrease the effects of the spurious velocities on the thermohydrodynamic of the multiphase system.

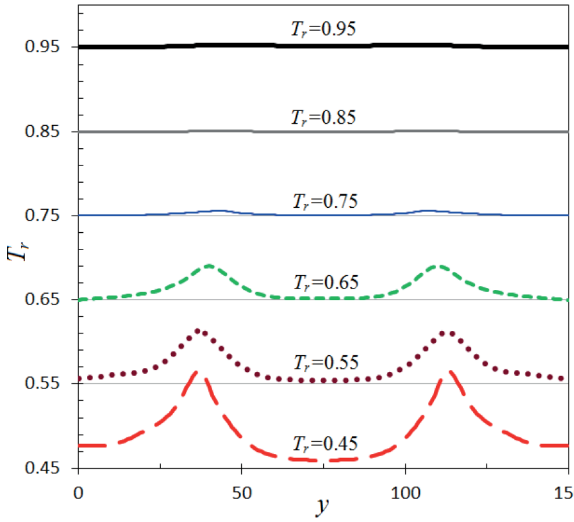

FIG. 18. (Color online) Temperature profile along the vertical centerline of the domain for different isothermal temperatures for $\tau = 0.8$.

ACKNOWLEDGMENTS

Helpful discussions with Professor Jos Derksen are gratefully acknowledged. This work was done as part of research sponsored by the Dutch Institute for Sustainable Process Technology (ISPT) and Shell, The Netherlands.

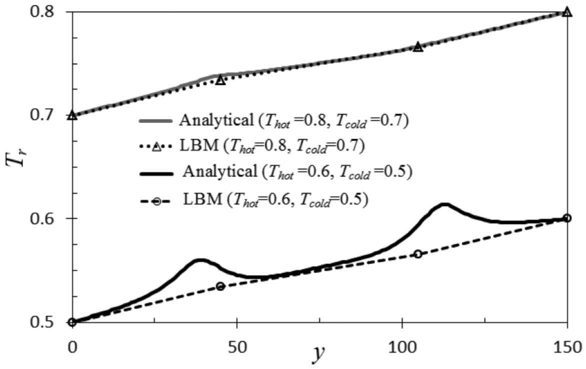

FIG. 19. Temperature profile along the vertical centerline of the nonisothermal domain for $\tau = 0.8$. Top plot: $T_{r,\text{hot}} = 0.8$ and $T_{r,\text{cold}} = 0.7$; lower plot: $T_{r,\text{hot}} = 0.6$ and $T_{r,\text{cold}} = 0.5$.

[1] H. S. Udaykumar, R. Mittal, and W. Shyy, J. Comput. Phys. **153**, 535 (1999).
[2] G. Tryggvason, B. Bunner, A. Esmaeeli, D. Juric, N. Al-Rawahi, W. Tauber, J. Han, S. Nas, and Y. J. Jan, J. Comput. Phys. **169**, 708 (2001).
[3] S. G. Yoon, Ph.D. thesis, Purdue University, 2002.
[4] B. J. Daly, Phys. Fluids **12**, 1340 (1969).
[5] C. W. Hirt and B. D. Nichols, J. Comput. Phys. **39**, 201 (1981).
[6] I. Chakraborty, G. Biswas, and P. S. Ghoshdastiar, Int. J. Heat Mass Tran. **58**, 240 (2013).
[7] M. K. Ikeda, P. Rao, and L. A. Schaefer, Comput. Fluids **101**, 250 (2014).
[8] J. Bao and L. Schaefer, Appl. Math. Model **37**, 1860 (2013).
[9] A. K. Gunstensen, D. H. Rothman, S. Zaleski, and G. Zanetti, Phys. Rev. A **43**, 4320 (1991).
[10] X. He, S. Chen, and R. Zhang, J. Comput. Phys. **152**, 642 (1999).
[11] M. R. Swift, W. R. Osborn, and J. M. Yeomans, Phys. Rev. Lett. **75**, 830 (1995).
[12] X. Shan and H. Chen, Phys. Rev. E **47**, 1815 (1993).
[13] X. Shan and H. Chen, Phys. Rev. E **49**, 2941 (1994).
[14] R. Nourgaliev, T. Dinh, T. Theofanous, and D. Joseph, Int. J. Multiphas. Flow **29**, 117 (2003).
[15] S. Hou, X. Shan, Q. Zou, G. D. Doolen, and W. E. Soll, J. Comput. Phys. **138**, 695 (1997).
[16] Z. Yu and L.-S. Fan, Phys. Rev. E **82**, 046708 (2010).
[17] L. Chen, Q. Kang, Y. Mua, Y. L. He, and W. Q. Tao, Int. J. Heat Mass Tran. **76**, 210 (2014).
[18] P. Yuan and L. Schaefer, Phys. Fluids **18**, 042101 (2006).
[19] A. L. Kupershtokh, D. A. Medvedev, and D. I. Karpov, Comput. Math. Appl. **58**, 965 (2009).
[20] M. Sbragaglia, R. Benzi, L. Biferale, S. Succi, K. Sugiyama, and F. Toschi, Phys. Rev. E **75**, 026702 (2007).
[21] S. Khajepor, J. Wen, and B. Chen, Phys. Rev. E **91**, 023301 (2015).
[22] Q. Li and K. H. Luo, Appl. Therm. Eng. **72**, 56 (2014).
[23] S. Gong and P. Cheng, Comput. Fluids **53**, 93 (2012).
[24] H. Huang, M. Krafczyk, and X. Lu, Phys. Rev. E **84**, 046710 (2011).
[25] Q. Li, K. H. Luo, and X. J. Li, Phys. Rev. E **86**, 016709 (2012).
[26] Q. Li, K. H. Luo, and X. J. Li, Phys. Rev. E **87**, 053301 (2013).
[27] K. Suna, T. Wang, M. Jia, and G. Xiao, Physica A **391**, 3895 (2012).
[28] Z. Yu and L.-S. Fan, J. Comput. Phys. **228**, 6456 (2009).
[29] M. Liu, Z. Yu, T. Wang, J. Wang, and L.-S. Fan, Chem. Eng. Sci. **65**, 5615 (2010).
[30] Z. Yu, H. Yang, and L.-S. Fan, Chem. Eng. Sci. **66**, 3441 (2011).
[31] M. R. Kamali, J. J. J. Gillissen, H. E. A. van den Akker, and S. Sundaresan, Phys. Rev. E **88**, 033302 (2013).
[32] A. Zarghami, S. Ubertini, and S. Succi, Comput. Fluids **77**, 56 (2013).
[33] X. Shan and G. D. Doolen, J. Stat. Phys. **81**, 379 (1995).
[34] M. R. Kamali and H. E. A. Van den Akker, Ind. Eng. Chem. Res. **52**, 11365 (2013).
[35] R. S. Qin, Phys. Rev. E **73**, 066703 (2006).
[36] X. Shan, Phys. Rev. E **73**, 047701 (2006).
[37] X. Shan, Phys. Rev. E **77**, 066702 (2008).
[38] S. Gong and P. Cheng, Int. J. Heat Mass Tran. **55**, 4923 (2012).
[39] X. He, Q. Zuo, and L.-S. Luo, J. Stat. Phys. **87**, 115 (1997).
[40] J. M. Buick and C. A. Greated, Phys. Rev. E **61**, 5307 (2000).
[41] Z. Guo, C. Zheng, and B. Shi, Phys. Rev. E **65**, 046308 (2002).
[42] D. Lycett-Brown and K. H. Luo, Phys. Rev. E **91**, 023305 (2015).
[43] T. L. Hill, *Statistical Thermodynamics* (Addison-Wesley, Boston, 1960).
[44] Y. S. Wei and R. J. Sadus, AICHE J. **46**, 169 (2000).
[45] N. Carnahan and K. Starling, J. Chem. Phys. **51**, 635 (1969).
[46] A. Zarghami, S. Ubertini, and S. Succi, Int. J. Numer. Method H. **24**, 270 (2014).
[47] A. A. Mohamad and A. Kuzmin, Int. J. Heat Mass Tran. **53**, 990 (2010).
[48] A. Hu, L. Li, S. Chen, Q. Liao, and J. Zeng, Int. J. Heat Mass Tran. **67**, 159 (2013).
[49] A. J. Wagner, Phys. Rev. E **74**, 056703 (2006).
[50] E. S. Kikkinides, A. G. Yiotis, M. E. Kainourgiakis, and A. K. Stubos, Phys. Rev. E **78**, 036702 (2008).
[51] M. Sbragaglia and D. Belardinelli, Phys. Rev. E **88**, 013306 (2013).
[52] J. K. Singh, J. Adhikari, and S. K. Kwak, Fluid Phase Equilibr. **248**, 1 (2006).